

High-fidelity SIM reconstruction-based super-resolution quantitative FRET imaging

Zewei Luo,^{a,b,†} Guodong Zang,^{a,b,†} Ge Wu,^{a,b} Mengting Kong,^{a,b} Zhengfei Zhuang,^{a,b} and Tongsheng Chen^{a,b,*}

^aSouth China Normal University, College of Biophotonics, MOE Key Laboratory of Laser Life Science, Guangzhou, China

^bSouth China Normal University, College of Biophotonics, Guangdong Key Laboratory of Laser Life Science, Guangzhou, China

Abstract. Structured illumination-based super-resolution Förster resonance energy transfer microscopy (SIM-FRET) provides an approach to resolving molecular behavior localized in intricate biological structures in living cells. However, SIM reconstruction artifacts will decrease the quantitative analysis fidelity of SIM-FRET signals. To address these issues, we have developed a method called HiFi spectrum optimization SIM-FRET (HiFi-SO-SIM-FRET), which uses optimized Wiener parameters in the two-step spectrum optimization to suppress sidelobe artifacts and achieve super-resolution quantitative SIM-FRET. We validated our method by demonstrating its ability to reduce reconstruction artifacts while maintaining the accuracy of FRET signals in both simulated FRET models and live-cell FRET-standard construct samples. In summary, HiFi-SO-SIM-FRET provides a promising solution for achieving high spatial resolution and reducing SIM reconstruction artifacts in quantitative FRET imaging.

Keywords: super-resolution structured illumination microscopy; Förster resonance energy transfer; living cells; quantitative measurement.

Received May 2, 2023; revised manuscript received Aug. 3, 2023; accepted for publication Aug. 18, 2023; published online Sep. 13, 2023.

© The Authors. Published by SPIE and CLP under a Creative Commons Attribution 4.0 International License. Distribution or reproduction of this work in whole or in part requires full attribution of the original publication, including its DOI.

[DOI: [10.1117/1.APN.2.5.056008](https://doi.org/10.1117/1.APN.2.5.056008)]

1 Introduction

Super-resolution (SR) microscopy has opened up new avenues for scientists to perform SR Förster resonance energy transfer (SR-FRET) imaging for exploring the molecular structure and function in intricate biological structures.^{1,2} Conventional FRET methods analyze the interaction between biomolecules by quantitatively measuring the FRET efficiency (E_D) and the concentration ratio of total acceptor to donor (R_C).^{3,4} While SR-FRET further reveals FRET signals of molecular interactions in subdiffraction regions, providing a deeper insight into intricate biological structures.^{5,6} Various research teams have implemented SR-FRET based on single-molecule localization microscopy and stimulated emission depletion microscopy, using fixed samples with photostable dyes during imaging.^{7–10} Our group has demonstrated that SR structured illumination microscopy (SR-SIM) can be combined with FRET to achieve SR-FRET. This method, called structured illumination-based

super-resolution Förster resonance energy transfer microscopy (SIM-FRET), enables dynamic SR quantitative FRET imaging of living cells.^{11,12} SIM-FRET achieves high spatiotemporal resolution and minimal photodamage while remaining compatible with commonly used fluorescent protein FRET pairs for conventional live-cell FRET imaging.^{12–14}

Although SIM-FRET has demonstrated its capability to quantify FRET analysis in living cells, the accuracy of quantitative analysis is still greatly affected by SIM reconstruction artifacts. To maintain the fidelity of image intensity, SIM-FRET has conventionally employed linear Wiener reconstruction for SR image reconstruction.^{15,16} However, the equivalent optical transfer function (OTF) of Wiener-SIM has raised peaks and downward kinks, which is different from the ideal OTF with doubled resolution.^{17,18} The non-smooth structure of this synthetic OTF causes reconstructed images to be affected by sidelobe artifacts and residual background fluorescence,^{19,20} which can result in incorrect FRET analysis results. Wen et al. developed a high-fidelity SIM reconstruction algorithm (HiFi-SIM) to address this issue.²¹ HiFi-SIM tackles the problem of fixed pattern and sidelobe artifacts in reconstructed images

*Address all correspondence to Tongsheng Chen, chentsh@scnu.edu.cn

[†]These authors contributed equally to this work.

by designing an effective point spread function (PSF) and optimizing it through a two-step spectrum optimization process, resulting in a reduction of background artifacts.^{22,23} However, directly applying HiFi-SIM to FRET analysis may introduce biased results due to inconsistent changes in the relative intensity values of the three channels.

Here, to reduce the impact of SIM reconstruction artifacts on SR-FRET and maintain image intensity fidelity, we have developed a two-step spectrum optimization algorithm for SIM-FRET that optimizes the Wiener parameters to suit the combination of HiFi-SIM reconstruction framework and FRET analysis. First, we conducted imaging experiments on various simulation models to verify the ability of HiFi spectrum optimization SIM-FRET (HiFi-SO-SIM-FRET) to remove artifacts and quantitatively measure FRET. Next, we evaluated the ability of HiFi-SO-SIM-FRET on live-cell FRET standard construction samples. Different results showed that the FRET efficiency (E_D) and the concentration ratio of total acceptor to donor (R_C) values measured in HiFi-SO-SIM-FRET were consistent with wide-field Förster resonance energy transfer (WF-FRET) imaging. In contrast, combining HiFi-SIM with FRET analysis without parameter optimization resulted in distorted FRET results. In summary, our results indicate that HiFi-SO-SIM-FRET can quantitatively analyze SIM-FRET signals and reduce SIM reconstruction artifacts in quantitative SR-FRET images.

2 Materials and Methods

2.1 Cell Culture, Plasmids, and Transfection

Michigan Cancer Foundation-7 (MCF-7) cells were purchased from the National Collection of Authenticated Cell Cultures (Shanghai, China) and cultured in Dulbecco's Modified Eagle's Medium (DMEM, Gibco, New York, United States), which contains 10% fetal calf serum (FBS, Gibco, New York, United States) and 1% Gentamicin–amphotericin B mixed solution (Leagene, Beijing, China) at 37°C under 5% CO₂ in a humidified incubator.

For plasmids, enhanced green fluorescent protein (EGFP) (#74165) and mCherry (#176016) plasmids were obtained from Addgene (Cambridge, Massachusetts, United States). The plasmid of mCherry-ActA was kindly provided by David W. Andrews. To generate a plasmid encoding green fluorescent protein (GFP) fused to ActA, the coding region for ActA was prepared by polymerase chain reaction (PCR) from the ActA complementary DNA (cDNA) of mCherry-ActA and replaced the BCL2 antagonist/killer 1 (Bak) coding region from the plasmid encoding GFP-Bak. The G17M-ActA construction was prepared in the G17M by replacing the stop codon with the ActA cloning region.

For transfection, MCF-7 cells were cultured in DMEM containing 10% fetal calf serum in a 20-mm glass dish at 37°C under 5% CO₂ in a humidified incubator. After 24 h, when the cells reached from 50% to 60% confluence, the plasmid was transfected into the MCF-7 cells for 24 to 48 h using TurbofectTM (Invitrogen) *in vitro* transfection reagent according to the manufacturer's standard protocol. We used living MCF-7 cells expressing GFP and mCherry separately to measure the spectral cross talk coefficients: a , b , c , d . The system calibration factors (G and k factors) were measured by implementing the mPb-G method with G17M and G32M;³ the statistical results from at least 20 living were a (0.0806 ± 0.0073),

b (0.0148 ± 0.0051), c (0.0667 ± 0.0021), d (0.1663 ± 0.0210), G (0.5815 ± 0.0898), and k (1.3449 ± 0.1362), respectively.

2.2 SIM Imaging

A multicolor, multidetection channel SIM system is used to obtain cell images, and the integrated microscope system mainly includes a microscope objective (APO TIRF 60× NA 1.49, Nikon), a multiwavelength laser (488 nm, donor-excited and 561 nm, receptor-excited), a spatial light modulator, a customized spatial mask, and a customized azimuthally patterned polarizer. The fluorescence emission light emitted by the specimen passed through a multiband dichroic mirror (DI03-R405/488/561/635, Semrock) as well as two bandpass emission filters. The donor emission filter (EM1, ET530/30x, Chroma) and acceptor emission filter (EM2, BA570-625, Olympus) were utilized. These emission filters were mounted in a fast motorized emission filter wheel (FW103, Thorlabs). Donor and acceptor lasers are calibrated at a uniform baseline, and the illumination power is adjusted in equal proportions so the FRET parameters are independent of the illumination power. To ensure synchronized and controlled operation of all the system components during image acquisition, a microcontroller (Arduino Uno board, Arduino) was utilized. Custom-developed software written in LabVIEW (National Instruments Inc.) facilitated the communication and coordination of the electrically controlled devices, enabling seamless acquisition of the raw images for three SIM-FRET channels. The imaging sequence involves capturing images for the DD channel first, followed by DA and AA channels in a sequential manner. Typically, the exposure time for each frame of the raw image is set to 20 ms.

2.3 Methods

SIM-FRET requires three channels of SR-SIM raw images for calculation: DD (donor excitation, donor emission), DA (donor excitation, acceptor emission), and AA (acceptor excitation, acceptor emission). The observed emission distribution of raw data collected in each channel can be described by the following formula:

$$D_{\theta,n}^X(r) = \left\{ S(r) \cdot \left[1 + m_{\theta}^X \cdot \cos \left[k_{\theta}^X \cdot r + \phi_{\theta}^X + \frac{2\pi(n-1)}{3} \right] \right] \right\} \otimes H^X(r) + N^X(r), \quad (1)$$

where subscripts θ ($=1, 2, 3$) and n ($=-1, 0, 1$) denote the indices of the sinusoidal illumination pattern orientation and phase shift, respectively, superscripts X ($=DD, DA, AA$) denote the indices of the FRET image channel, $S(r)$ denotes the distribution of the samples, m_{θ}^X , k_{θ}^X , and ϕ_{θ}^X are the modulation depth, pattern wave vector, and initial phase of the sinusoidal illumination pattern, respectively, $H^X(r)$ is the PSF for different channels of the optical system, and $N^X(r)$ is additive Gaussian (white) noise.²⁴

In the previous SIM-FRET method, we employed linear Wiener reconstruction introduced by Gustaffson and Heintzmann.^{25,26} The reconstructed SR-SIM images [$I_{\text{Wiener}}^{\text{DD}}(r)/I_{\text{Wiener}}^{\text{AA}}(r)/I_{\text{Wiener}}^{\text{DA}}(r)$] for each channel are implemented by formulas as follows:

$$\begin{bmatrix} \tilde{S}_{\theta,0}^X(k) \\ \tilde{S}_{\theta,-1}^X(k - p_\theta^X) \\ \tilde{S}_{\theta,1}^X(k + p_\theta^X) \end{bmatrix} = \begin{bmatrix} 1 & m_\theta^X e^{-i(\phi_\theta^X)/2} & m_\theta^X e^{i(\phi_\theta^X)/2} \\ 1 & m_\theta^X e^{-i(\phi_\theta^X + \frac{2\pi}{3})/2} & m_\theta^X e^{i(\phi_\theta^X + \frac{2\pi}{3})/2} \\ 1 & m_\theta^X e^{-i(\phi_\theta^X + \frac{4\pi}{3})/2} & m_\theta^X e^{i(\phi_\theta^X + \frac{4\pi}{3})/2} \end{bmatrix}^{-1} \times \begin{bmatrix} \tilde{D}_{\theta,0}^X(k) \\ \tilde{D}_{\theta,-1}^X(k) \\ \tilde{D}_{\theta,1}^X(k) \end{bmatrix}, \quad (2)$$

$$\tilde{S}_{\text{directly-combined}}^X(k) = \sum_{\theta=1}^3 [\tilde{S}_{\theta,0}^X(k) \tilde{H}^*(k) + \tilde{S}_{\theta,+1}^X(k) \tilde{H}^*(k + k_\theta^X) + \tilde{S}_{\theta,-1}^X(k) \tilde{H}^*(k - k_\theta^X)], \quad (3)$$

$$W_{\text{Wiener}}^X(k) = \frac{\tilde{A}(k)}{\left\{ \sum_{\theta=1}^3 [|\tilde{H}^X(k)|^2 + |\tilde{H}^X(k + k_\theta^X)|^2 + |\tilde{H}^X(k - k_\theta^X)|^2] \right\} + w^2}, \quad (4)$$

$$I_{\text{Wiener}}^X(r) = \text{ifft}[\tilde{S}_{\text{directly-combined}}^X(k) \cdot W_{\text{Wiener}}^X(k)], \quad (5)$$

where $\tilde{D}_{\theta,n}^X(k)$ represents the Fourier domain of the raw SIM-FRET channel images $D_{\theta,n}^X(r)$, $\tilde{S}_{\theta,0}^X(k)$ and $\tilde{S}_{\theta,\pm 1}^X(k)$ are the 0th-order and ± 1 st-order separated components, $\tilde{H}^X(k)$ is the OTF of the SIM-FRET channel, $\tilde{A}(k)$ is the apodization function, and w is the Wiener parameter. To ensure a consistent relative intensity relationship among the three channels while extending the frequency spectrum, a unified Wiener parameter and Gaussian-shaped apodization function $\tilde{A}(k) = \exp[-0.5(k\sqrt{2 \ln 2})^2]$ are applied to the three-channel SIM-FRET image reconstruction, with the Wiener parameter empirically adjusted to 0.2.

The HiFi-SIM reconstruction algorithm addresses the mismatch between the equivalent OTF and the ideal SR OTF using a two-step spectrum optimization approach, resulting in reduced sidelobe artifacts in the image. The composite filter of HiFi-SIM can be represented by the following formula:²¹

$$W_{\text{HiFi}}^X(k) = \frac{\tilde{H}_{\text{ideal}}(k)}{\left[\sum_m a_1(k + mk_d) \cdot |\tilde{H}(k + mk_d)|^2 + w_1^2 \right]} \cdot \frac{\tilde{A}(k)}{\left[\sum_m a_2(k + mk_d) \cdot |\tilde{H}(k + mk_d)|^2 + w_2^2 \right]}, \quad (6)$$

where $\tilde{H}_{\text{ideal}}(k)$ represents an ideal OTF with the double resolution, w_1 and w_2 represent empirical parameters for Wiener deconvolution, empirically adjusted to 1.2 and 0.2 in three-channel SIM-FRET image reconstruction, and $a_1(k)$ and $a_2(k)$ are the attenuation function that can be expressed by the following formulas:

$$a_1(k) = \begin{cases} 1 - S_{\text{att}} e^{-\frac{k^2}{(0.5 \cdot W_{\text{att}})^2}}, & m = \pm 1, \\ 1, & m = 0 \end{cases}, \quad (7)$$

$$a_2(k) = \begin{cases} 1 - \frac{S_{\text{att}}}{1.15} e^{-\frac{k^2}{(0.5 \cdot W_{\text{att}})^2}}, & m = \pm 1, \\ 1 - \frac{S_{\text{att}}}{1.05} e^{-\frac{k^2}{(0.5 \cdot W_{\text{att}})^2}}, & m = 0 \end{cases}, \quad (8)$$

where S_{att} and W_{att} are the attenuation strength and width, respectively.

From Figs. 1(b) and 1(d), it can be observed that the composite filter used in HiFi-SIM differs significantly from the filter used in Wiener-SIM in the frequency domain. This spectral optimization in HiFi-SIM's composite filter reflects its mechanism for eliminating sidelobe artifacts. However, when combining HiFi-SIM with FRET analysis on images captured with different OTF channels (in FRET three-channel imaging, the donor emission channel has an emission center wavelength of 525 nm, and the acceptor emission channel has an emission center wavelength of 600 nm), we found that the ratio of the composite filter in HiFi-SIM was inconsistent with the Wiener filter in the acceptor and donor channels [Fig. 1(c)]. As a result, the relative intensity values of the FRET three-channel images exhibited inconsistent variations. Previous methodologies used Wiener-SIM with uniform reconstruction parameters to ensure consistent variations in the reconstructed image intensities for all three channels. However, HiFi-SIM with uniform reconstruction parameters does not maintain consistent variations in the reconstructed image intensities for all three channels [Fig. 1(d)]. To minimize the bias introduced by combining HiFi-SIM with FRET analysis, we developed a parameter optimization method to automatically adjust the two Wiener parameters in the HiFi-SIM composite filter to reduce the difference in the reconstruction intensity ratio between the DD channel and the DA and AA channels in SIM-FRET reconstruction between HiFi-SIM and conventional Wiener-SIM. The optimal Wiener parameters can be calculated using the following formula:

$$\{\hat{w}_1, \hat{w}_2\} = \underset{w_1, w_2}{\text{argmin}} \left(\frac{W_{\text{Wiener}}^{\text{AA}}(w)}{W_{\text{Wiener}}^{\text{DD}}(w)} - \frac{W_{\text{HiFi}}^{\text{AA}}(w_1, w_2)}{W_{\text{HiFi}}^{\text{DD}}(w_1, w_2)} \right). \quad (9)$$

Using the optimized \hat{w}_1 and \hat{w}_2 , each channel of the HiFi-SO-SIM retains the characteristics of the HiFi-SIM composite filter, attaining the identical effect of sidelobe artifact removal as HiFi-SIM while the ratio of the two channels is close to that of the Wiener-SIM composite filter [Fig. 1(c)], approaching the fidelity of Wiener-SIM in terms of intensity fidelity. The optimized values of \hat{w}_1 and \hat{w}_2 are brought into Eq. (6) to obtain a new composite filter, and then the SIM image is reconstructed according to following formulas:

$$W_{\text{SO-SIM}}^X(k) = \frac{\tilde{H}_{\text{ideal}}(k)}{\left[\sum_m a_1(k + mk_d) \cdot |\tilde{H}(k + mk_d)|^2 + \hat{w}_1^2 \right]} \cdot \frac{\tilde{A}(k)}{\left[\sum_m a_2(k + mk_d) \cdot |\tilde{H}(k + mk_d)|^2 + \hat{w}_2^2 \right]}, \quad (10)$$

$$I_{\text{SO-SIM}}^X(r) = \text{ifft}\{[\tilde{S}_{\text{directly-combined}}^X(k) \cdot W_{\text{SO-SIM}}^X(k)]\}. \quad (11)$$

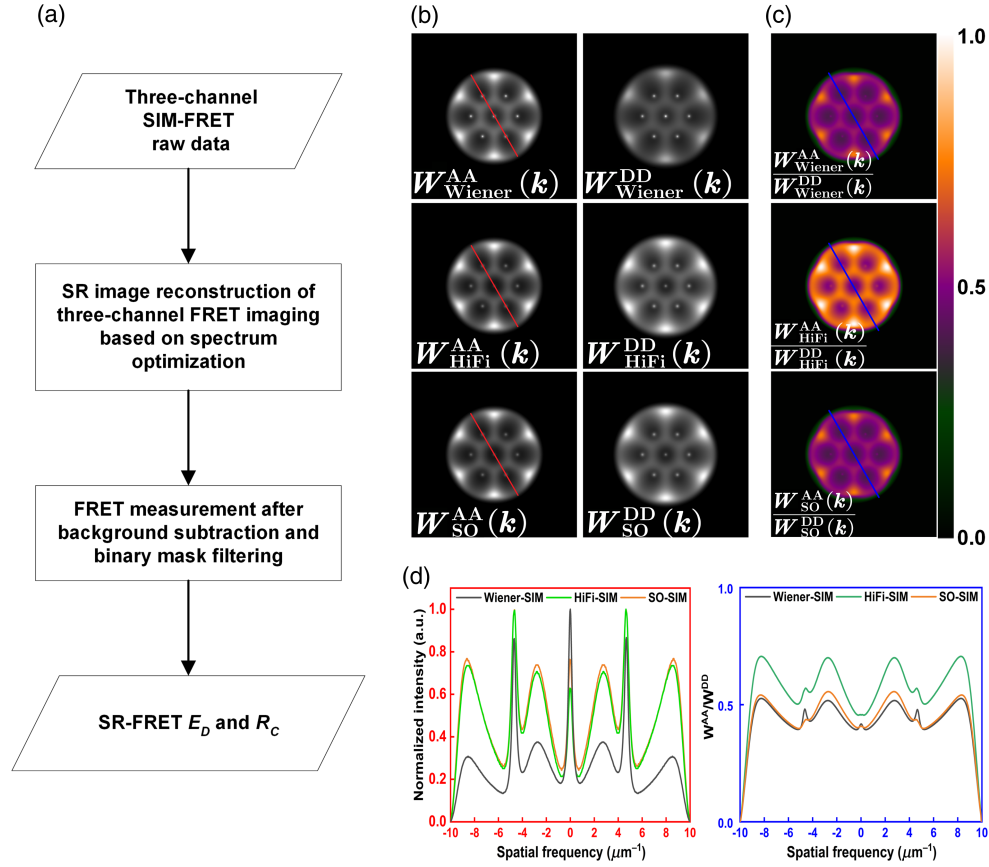


Fig. 1 Flow chart and basic principle of HiFi-SO-SIM-FRET. (a) The HiFi-SO-SIM-FRET flow chart includes obtaining three-channel FRET structured illumination modulated raw image stacks, SR-SIM image reconstruction of the three-channel FRET imaging based on spectrum optimization, background subtraction, binary mask filtering, and quantitative sensitized emission FRET measurement. (b) Composite filter for acceptor (AA) and donor (DD) channels of Wiener-SIM, HiFi-SIM, and HiFi-SO-SIM. (c) Composite filter ratio of acceptor and donor channels for Wiener-SIM, HiFi-SIM, and HiFi-SO-SIM. (d) Intensity profiles of the red lines in panel (b) and intensity profiles of the blue lines in panel (c).

The background of the reconstructed three-channel SR-FRET image is removed based on the average intensity of the background region in each image and then designs a binary mask filter.²⁷ Then, the donor-centric FRET efficiency (E_D) and the concentration ratio of total acceptor to donor (R_C) are measured by following equations:^{28,29}

$$E_D = \frac{F_C}{F_C + G \cdot I_{SIM}^{DD}}, \quad (12)$$

$$R_C = \frac{k \cdot I_{SIM}^{AA}}{F_C/G + I_{SIM}^{DD}}, \quad (13)$$

where G is the sensitivity quenching factor and k is the concentration correction factor. G and k can be determined experimentally using a specific construct with a donor-acceptor ratio of 1:1.³ I_{SIM}^{DD} is the donor intensity in donor channel with donor excitation; I_{SIM}^{AA} is the acceptor intensity in acceptor channel with acceptor excitation; F_C is the acceptor-sensitized emission in the acceptor channel calculated as follows:³⁰

$$F_C = I_{SIM}^{DA} - a(I_{SIM}^{AA} - c \cdot I_{SIM}^{DD}) - d(I_{SIM}^{DD} - b \cdot I_{SIM}^{AA}), \quad (14)$$

where I_{SIM}^{DA} is the fluorescence intensity in the acceptor channel with donor excitation; a , b , c , and d are spectral cross talk calibration coefficients that can be predetermined using donor-only and acceptor-only specimens.

The flow chart of HiFi-SO-SIM-FRET is shown in Fig. 1(a). Overall, the following steps are required to implement HiFi-SO-SIM-FRET: (1) reconstructing structured illuminated raw image stacks of three FRET channels based on spectrum optimization to obtain SR images and (2) quantitative calculation of FRET efficiency (E_D) and the concentration ratio of total acceptor to donor (R_C) from reconstructed SR images via a three-channel postprocessing process, including background subtraction and binary mask filtering.

3 Results

3.1 Performance in Simulated Models

First, to validate that HiFi-SO-SIM-FRET can reduce sidelobe artifacts in reconstructed images and eliminate the effects of sidelobe artifacts on quantitative FRET, we conducted experiments on simulated structural images to demonstrate the

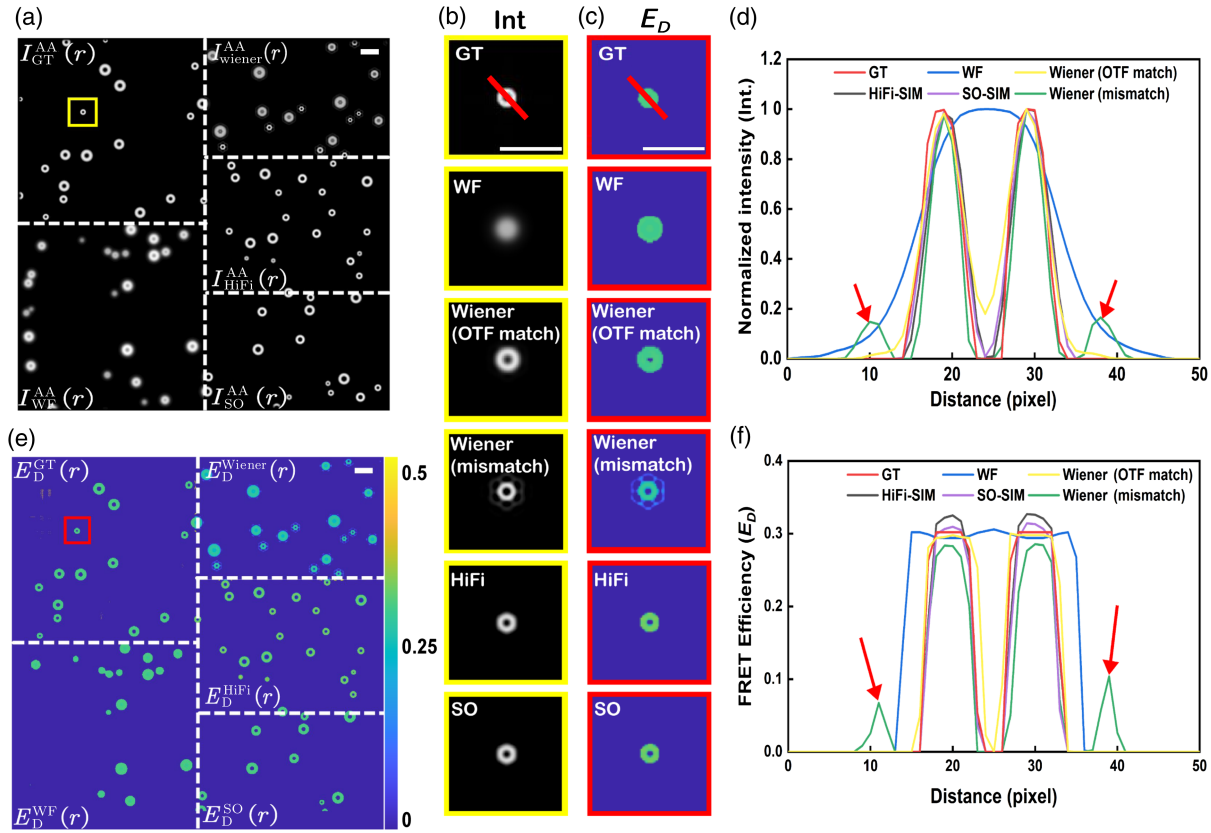


Fig. 2 Feasibility of HiFi-SO-SIM for the elimination of sidelobe artifacts and quantitative calculation of FRET. (a) GT of simulated rings, WF imaging, and corresponding SR images reconstructed by Wiener-SIM, HiFi-SIM, and HiFi-SO-SIM. (b) Magnified images of the GT, WF, Wiener-SIM, HiFi-SIM, and HiFi-SO-SIM results corresponding to the yellow-boxed region in panel (a). (c) Magnified images of the GT, WF, Wiener-SIM, HiFi-SIM, and HiFi-SO-SIM results corresponding to the red-boxed region in panel (e). (d) Intensity profiles of the red lines in panel (b). Red arrows indicate sidelobe artifacts produced by OTF mismatch. (e) FRET E_D images of GT, WF, Wiener-SIM, HiFi-SIM, and HiFi-SO-SIM. (f) E_D profiles of the red lines in panel (c). Red arrows indicate the erroneous FRET signals generated by sidelobe artifacts. Scale bar: 50 pixels.

effectiveness of our method. Specifically, the simulated ring pattern was generated by fairSIM with an image size of 512 pixels, and the diameter of the circles distributed in the image was from 50 to 150 nm.¹⁵ Ground truth (GT) predetermined the FRET efficiency ($E_D = 0.3$) and the concentration ratio of total acceptor to donor ($R_C = 1$). The stack of SIM-FRET raw images with three channels was generated using the SR-SIM general forward imaging model shown in Eq. (1). Notably, we obtained the simulated three-channel FRET raw image stacks by Eq. (1), where $H^X(r)$ is the measured PSF of the system, and the PSF has been experimentally measured using 100 nm fluorescent microspheres (0.1 μm TetraSpeck Microspheres, T7279, Thermofisher). The cross talk coefficient was assumed to be $a = 0.2$, $b = 0$, $c = 0$, $d = 0.8$, $G = 5$, and $k = 0.69$. The pixel size used for the simulation was 6.5 μm . The assumed emission wavelength for the DD channel was 525 nm, the assumed wavelength for the DA and AA channels was 600 nm, and the numerical aperture was 1.49. We compared the reconstructed HiFi-SO-SIM images with wide-field (WF), Wiener-SIM, and HiFi-SIM. The imaging results of different methods are shown in Fig. 2(a). As can be seen in Fig. 2(b), the WF results could not distinguish the circular structure, and the Wiener-SIM

reconstructed image showed significant snowflake-like artifacts around the ring, which was caused by the OTF mismatch. These artifacts were visible in the line profiles [Fig. 2(d), indicated by red arrows]. In contrast, both HiFi-SO-SIM and HiFi-SIM could suppress these artifacts, resulting in a cleaner hollow ring structure. In terms of quantitative FRET, Fig. 2(e) shows the pseudocolor map of FRET efficiency for GT, WF, Wiener-SIM, HiFi-SIM, and HiFi-SO-SIM. Snowflake artifacts could lead to incorrect FRET signals, as shown in Fig. 2(c). These FRET signals were visible in the line profiles [Fig. 2(f), indicated by red arrows]. The Wiener-SIM reconstructed image produced incorrect FRET efficiency, while HiFi-SO-SIM and HiFi-SIM could eliminate this misinformation [Fig. 2(f)]. On the other hand, the FRET efficiency obtained by HiFi-SO-SIM-FRET was closer to the GT value and was not affected by sidelobe artifacts while the FRET efficiency obtained by HiFi-SIM is significantly higher [Fig. 2(f)].

Next, to verify the capability of HiFi-SO-SIM to reduce bias in HiFi-SIM quantitative FRET calculations, we conducted experiments on the star pattern simulation. We conducted experiments on the simulated star pattern using the same imaging process and coefficients as for the simulated ring pattern, but

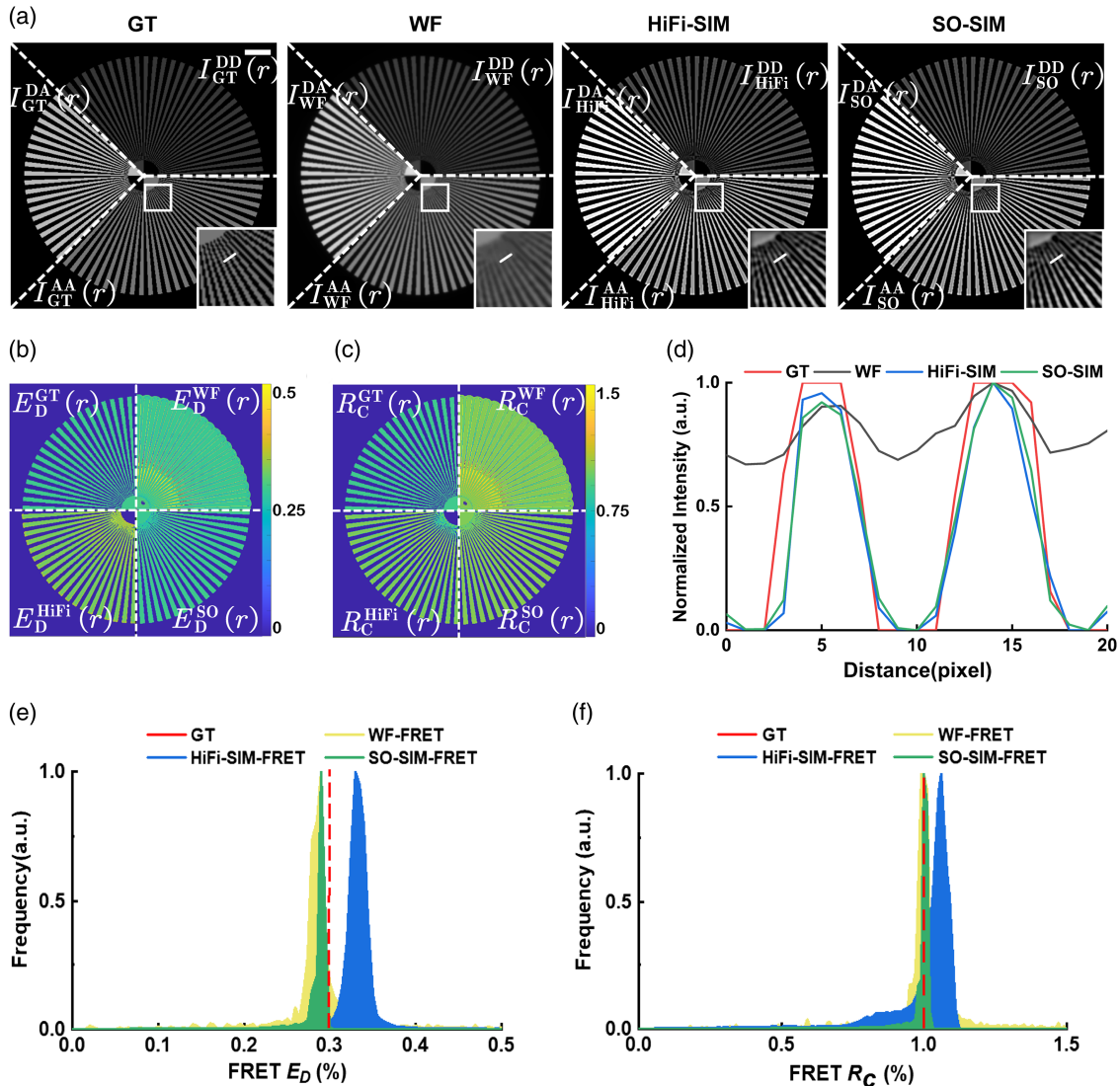


Fig. 3 Performance of HiFi-SO-SIM in FRET star-like pattern simulation. (a) Three-channel images of simulation FRET models of GT, WF, HiFi-SIM, and HiFi-SO-SIM. (b) FRET E_D images of GT, WF, HiFi-SIM, and HiFi-SO-SIM. (c) FRET R_C images of GT, WF, HiFi-SIM, and HiFi-SO-SIM. (d) Intensity profiles of the white solid lines in panel (a). (e) Corresponding histograms of E_D in panel (b). (f) Corresponding histograms of R_C in panel (c). Scale bar: 100 pixels.

the OTF of the imaging process was replaced by the theoretical simulated OTF to avoid OTF mismatch, with parameters set to match the microscope and the three-channel FRET emission wavelength. The GT consisted of a synthetic star pattern formed by a predetermined FRET efficiency ($E_D = 0.3$) and the concentration ratio of total acceptor to donor ($R_C = 1$). Figure 3(a) shows the three-channel images of GT, WF, HiFi-SIM, and HiFi-SO-SIM. Further, Fig. 3(b) shows the pseudo-color map of FRET efficiency for each method, and Fig. 3(c) shows the corresponding FRET R_C pseudo-color maps. Figure 3(d) shows that HiFi-SO-SIM could provide the same high lateral resolution as HiFi-SIM and distinguish structures that WF could not distinguish. Figure 3(e) shows the histograms of E_D and R_C for different methods. We additionally performed line analysis along the axes of the Siemens star pattern in Fig. 3(b). This analysis was conducted to analyze the FRET results of various reconstruction methods in low-frequency, mid-frequency, and

high-frequency spatial distributions. The results show that the FRET values reconstructed directly with HiFi-SIM and Wiener-SIM may deviate from the linear relationship with the GT in some regions or features (Fig. S1 in the [Supplementary Material](#)). It was noticeable that the E_D and R_C measured by HiFi-SO-SIM-FRET were closer to the GT than those measured by HiFi-SIM, which verifies the capability of HiFi-SO-SIM to reduce bias in HiFi-SIM quantitative FRET calculations [Fig. 3(e) and Fig. S1 in the [Supplementary Material](#)].

3.2 SR Live-Cell Quantitative FRET Imaging

To evaluate the capabilities of HiFi-SO-SIM-FRET in live cells, we conducted live-cell quantitative FRET experiments using the mitochondrial outer membrane (MOM)-targeted FRET standard construct, ActA-G17M, which has a predetermined FRET efficiency ($E_D = 0.2$) and a concentration ratio of total acceptor to

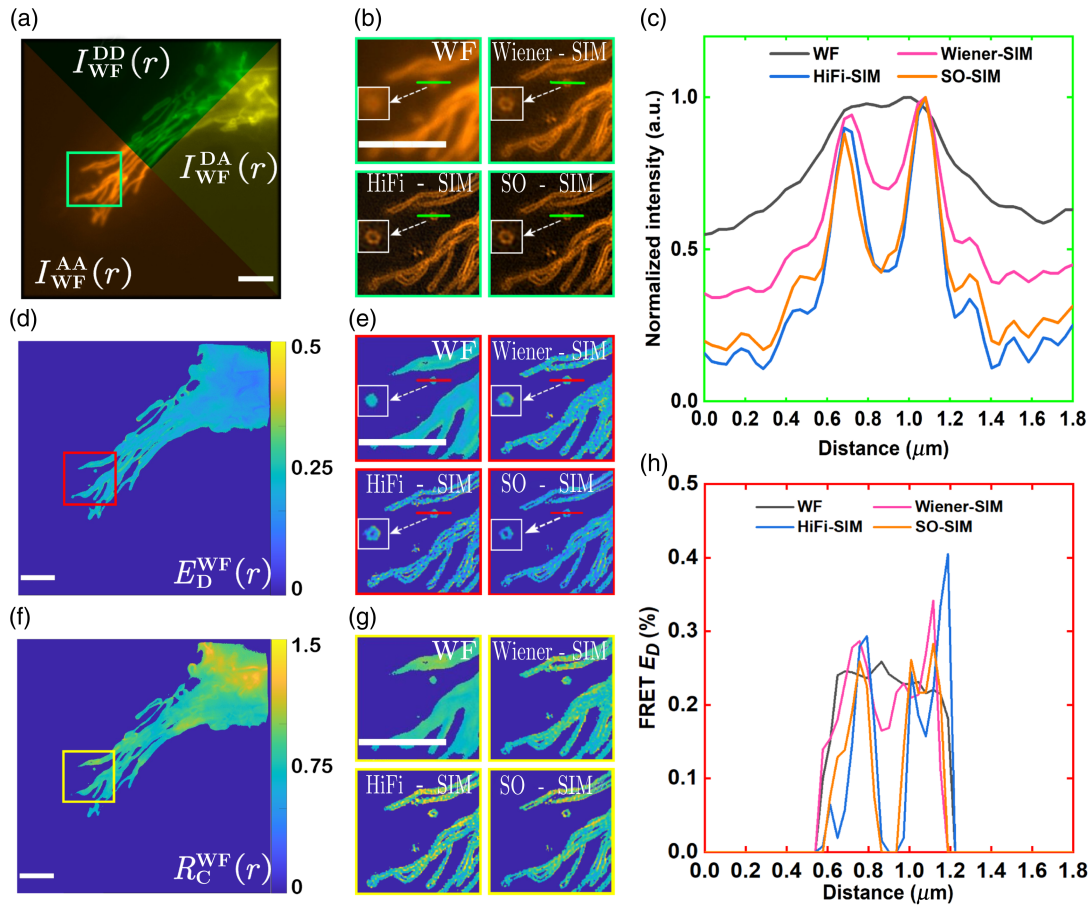


Fig. 4 Performance of HiFi-SO-SIM for quantitative FRET measurements in live cells. (a) Three-channel intensity WF images of ActA-G17M. (b) WF, Wiener-SIM, HiFi-SIM, and HiFi-SO-SIM magnified images of the green box area in the corresponding panel (a). (c) Intensity profiles of the green line in panel (b). (d) Pseudo-color images of WF E_D using raw three-channel images. (e) WF, Wiener-SIM, HiFi-SIM, and HiFi-SO-SIM magnified images of the red box area in the corresponding panel (d). (f) Pseudo-color images of WF R_C using raw three-channel images. (g) WF, Wiener-SIM, HiFi-SIM, and HiFi-SO-SIM magnified images of the yellow box area in the corresponding panel (f). (h) E_D profiles of the red lines in panel (e). Scale bar: 5 μm .

donor ($R_C = 1$). Spectral cross talk coefficients (a, b, c, d) were measured using live MCF-7 cells expressing GFP and mCherry separately. The reconstructed three-channel SIM-FRET images using HiFi-SO-SIM were subjected to FRET calculations, and the results were compared with those obtained through WF, Wiener-SIM, and HiFi-SIM. Figure 4(a) shows the representative three-channel WF intensity image of ActA-G17M. In the WF image, the circular structure around the MOM cannot be distinguished, and all SR images were significantly improved in lateral resolution, but the images obtained by Wiener-SIM were affected by the high background [Fig. 4(b)]. In the SR images obtained by HiFi-SIM and HiFi-SO-SIM, the background fluorescence inside and around the circular structure was well suppressed, and a clearer image of the circular spatial structure was obtained [Figs. 4(b) and 4(c)]. From reconstructed SIM-FRET three-channel images obtained by different methods, we calculated the corresponding pseudo-color images of E_D and R_C [Figs. 4(d)–4(h)]. The FRET signals that could not be distinguished in WF images were resolved in SR images while Wiener-SIM was affected by the background fluorescence, producing false FRET signals within the annulus. HiFi-SO-SIM

and HiFi-SIM could finely distinguish FRET signals by suppressing background fluorescence [Figs. 4(e) and 4(h)], and consistent with the results of the simulation experiments, the E_D obtained by HiFi-SIM was significantly biased [Fig. 4(h)].

Finally, we calculated the E_D and R_C of images from at least 15 fields of view using four methods; the statistical results are shown in Fig. 5. Notably, the statistical E_D and R_C values for HiFi-SO-SIM-FRET were closer to those obtained using WF compared with HiFi-SIM (Fig. 5), further validating the accuracy of our method for quantitative FRET calculation.

4 Discussion

In a previous study, we developed a SIM-FRET method enabling quantitative SR-FRET analysis in live cells.¹¹ However, Wiener-SIM for image reconstruction caused SIM-FRET to suffer from sidelobe artifacts due to inherent deficiencies in the synthetic OTF. In this paper, we present an improved SIM-FRET method based on spectrum optimization of the HiFi-SIM reconstruction framework (HiFi-SO-SIM-FRET). This approach significantly reduces sidelobe artifacts in SR-FRET

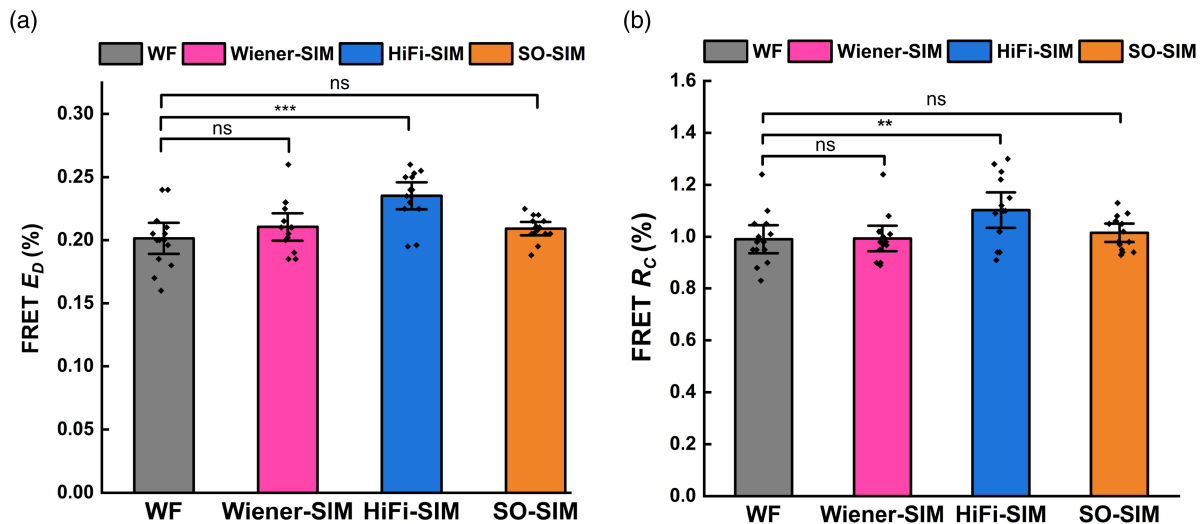


Fig. 5 Comparison of statistical E_D and R_C values using different methods. (a) Statistical E_D values using different methods. (b) Statistical R_C values using different methods. The unpaired student's t -test is used for data [(a) and (b)]. **, $p < 0.01$; ***, $p < 0.001$; ns, $p > 0.05$.

images and outperforms traditional Wiener-SIM, providing accurate quantitative analysis. HiFi-SIM does not maintain consistent variations in the reconstructed fluorescence signal intensity for FRET three channels, potentially leading to biased results. To address this issue, we optimized the Wiener parameter in HiFi-SIM through the ratio of Wiener-SIM filters in different channels. This parameter optimization method achieves reconstructed images of the same quality as HiFi-SIM and reduces bias in quantitative FRET analysis, obtaining results consistent with WF-FRET imaging.

On the other hand, due to the insensitivity of the HiFi-SIM algorithm to OTF mismatch and user-defined parameters, it is possible to use artificially set consistent OTF values for all three channels during HiFi-SIM reconstruction when combining it with FRET. To verify the feasibility of this approach, we compared the FRET results obtained from HiFi-SIM reconstruction under three scenarios: three-channel OTF matching, donor channel OTF mismatch, and acceptor channel OTF mismatch using both simulated and experimental data. The experimental results demonstrated that HiFi-SIM indeed exhibited parameter insensitivity, as the reconstructed three-channel images did not introduce artifacts due to OTF mismatch. However, the quantitative analysis results of E_D and R_C in FRET still did not match with prior reference values (Figs. S2 and S3 in the [Supplementary Material](#)). Our method preserves the relative gray-scale relationship of FRET three-channel images during HiFi-SIM reconstruction, leading to FRET results that are closer to GT values.

As an enhancement to the SIM-FRET method, HiFi-SO-SIM-FRET generates SIM-FRET images with reduced artifacts. However, this technique is susceptible to random artifact amplification caused by noise and fixed-pattern artifacts due to out-of-focus background in original images with a low signal-to-noise ratio (SNR) or high out-of-focus background. Chu et al.³¹ have developed an image reconstruction algorithm to process low-SNR raw images and reduce photobleaching and phototoxicity caused by illumination based on total variational constraints. This algorithm can reconstruct low SNR images into SR images

with the same resolution as images with a high SNR. Integrating this SIM reconstruction algorithm with quantitative FRET analysis can more effectively resolve image reconstruction challenges from low SNR, broadening the applicability of SIM-FRET.

In summary, HiFi-SO-SIM-FRET offers an effective solution to achieve high spatial resolution and decrease SIM artifacts in SR quantitative SIM-FRET imaging. Using optimized Wiener parameter selection, quantitative HiFi-SO-SIM-FRET is capable of reducing the deviation of HiFi-SIM-FRET results and SIM artifacts in SR imaging. The implementation of quantitative HiFi-SO-SIM-FRET can significantly enhance our comprehension of living cell processes by precisely quantifying dynamic molecular interactions within complex biological structures. This technology will broaden the application of quantitative SR-FRET in living cells.

Data Availability

Data underlying the results presented in this paper are not publicly available at this time but may be obtained from the authors upon request.

Acknowledgments

We thank Prof. Hui Li and Dr. Gang Wen at Suzhou Institute of Biomedical Engineering and Technology (SIBET) of the Chinese Academy of Sciences (CAS) for their valuable comments and suggestions. The work was supported by the National Natural Science Foundation of China (Grant No. 62135003) and Key-Area Research and Development Program of Guangdong Province (Grant No. 2022B0303040003).

References

1. A. M. Szalai, C. Zaza, and F. D. Stefani, "Super-resolution FRET measurements," *Nanoscale* **13**(44), 18421–18433 (2021).
2. L. A. Masullo et al., "Fluorescence nanoscopy at the sub-10 nm scale," *Biophys. Rev.* **13**, 1101–1112 (2021).

3. J. Zhang et al., “Reliable measurement of the FRET sensitized-quenching transition factor for FRET quantification in living cells,” *Micron* **88**, 7–15 (2016).
4. T. Zal and N. R. J. Gascoigne, “Photobleaching-corrected FRET efficiency imaging of live cells,” *Biophys. J.* **86**(6), 3923–3939 (2004).
5. A. Szabo et al., “Quo vadis FRET? Förster’s method in the era of superresolution,” *Methods Appl. Fluoresc.* **8**(3), 032003 (2020).
6. H. E. Grecco and P. J. Verveer, “FRET in cell biology: still shining in the age of super-resolution?” *ChemPhysChem*. **12**(3), 484–490 (2011).
7. A. Auer et al., “Fast, background-free DNA-PAINT imaging using FRET-based probes,” *Nano Lett.* **17**(10), 6428–6434 (2017).
8. S. Cho et al., “Simple super-resolution live-cell imaging based on diffusion-assisted Förster resonance energy transfer,” *Sci. Rep.* **3**, 1208 (2013).
9. H. Wallrabe and A. Periasamy, “Imaging protein molecules using FRET and FLIM microscopy,” *Anal. Biotechnol.* **16**(1), 19–27 (2005).
10. A. M. Szalai et al., “Super-resolution imaging of energy transfer by intensity-based STED-FRET,” *Nano Lett.* **21**(5), 2296–2303 (2021).
11. Z. Luo et al., “Structured illumination-based super-resolution live-cell quantitative FRET imaging,” *Photon. Res.* **11**(5), 887–896 (2023).
12. Z. Liu et al., “Optical section structured illumination-based Förster resonance energy transfer imaging,” *Cytometry A* **101**(3), 264–272 (2022).
13. A. Markwirth et al., “Video-rate multi-color structured illumination microscopy with simultaneous real-time reconstruction,” *Nat. Commun.* **10**(1), 4315 (2019).
14. S. Tu et al., “Fast reconstruction algorithm for structured illumination microscopy,” *Opt. Lett.* **45**(6), 1567–1570 (2020).
15. M. Müller et al., “Open-source image reconstruction of super-resolution structured illumination microscopy data in ImageJ,” *Nat. Commun.* **7**, 10980 (2016).
16. M. G. Gustafsson et al., “Three-dimensional resolution doubling in wide-field fluorescence microscopy by structured illumination,” *Biophys. J.* **94**(12), 4957–4970 (2008).
17. D. Li et al., “Extended-resolution structured illumination imaging of endocytic and cytoskeletal dynamics,” *Science* **349**, aab3500 (2015).
18. Y. Wu and H. Shroff, “Faster, sharper, and deeper: structured illumination microscopy for biological imaging,” *Nat. Methods* **15**(12), 1011–1019 (2018).
19. J. Demmerle et al., “Strategic and practical guidelines for successful structured illumination microscopy,” *Nat. Protoc.* **12**(5), 988–1010 (2017).
20. J. Fan et al., “A protocol for structured illumination microscopy with minimal reconstruction artifacts,” *Biophys. Rep.* **5**, 80–90 (2019).
21. G. Wen et al., “High-fidelity structured illumination microscopy by point-spread-function engineering,” *Light Sci. Appl.* **10**(1), 70 (2021).
22. Z. Wang et al., “Rapid, artifact-reduced, image reconstruction for super-resolution structured illumination microscopy,” *Innovation* **4**(3), 100425 (2023).
23. G. Wen et al., “Frequency–spatial domain joint optimization for improving super-resolution images of nonlinear structured illumination microscopy,” *Opt. Lett.* **46**(23), 5842–5845 (2021).
24. A. Lal, C. Shan, and P. Xi, “Structured illumination microscopy image reconstruction algorithm,” *IEEE J. Sel. Top. Quantum Electron.* **22**(4), 50–63 (2016).
25. M. G. L. Gustafsson, “Surpassing the lateral resolution limit by a factor of two using structured illumination microscopy,” *J. Microsc.* **198**(2), 82–87 (2000).
26. R. Heintzmann and C. G. Cremer, “Laterally modulated excitation microscopy: improvement of resolution by using a diffraction grating,” *Proc. SPIE* **3568**, 185–196 (1999).
27. C. Zhang et al., “Automated E-FRET microscope for dynamical live-cell FRET imaging,” *J. Microsc.* **274**(1), 45–54 (2019).
28. M. Ben-Johny, D. N. Yue, and D. T. Yue, “Detecting stoichiometry of macromolecular complexes in live cells using FRET,” *Nat. Commun.* **7**, 13709 (2016).
29. F. Yang et al., “Stoichiometry and regulation network of Bcl-2 family complexes quantified by live-cell FRET assay,” *Cell. Mol. Life Sci.* **77**(12), 2387–2406 (2020).
30. H. Chen et al., “Measurement of FRET efficiency and ratio of donor to acceptor concentration in living cells,” *Biophys. J.* **91**(5), L39–L41 (2006).
31. K. Chu et al., “Image reconstruction for structured-illumination microscopy with low signal level,” *Opt. Express* **22**(7), 8687–8702 (2014).

Biographies of the authors are not available.